Heliyon 10 (2024) e26680

Contents lists available at ScienceDirect

Heliyon

journal homepage: www.cell.com/heliyon

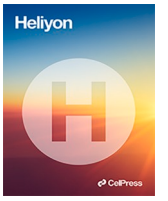

Research article

Poly(p-phenylene)-based membranes with cerium for chemically durable polymer electrolyte fuel cell membranes

Abdul Kodir [a,b], Seunghee Woo [b], Sang-Hun Shin [c], Soonyong So [c], Duk Man Yu [c], Hyejin Lee [b], Dongwon Shin [a,b], Jang Yong Lee [c], Seok-Hee Park [b], Byungchan Bae [a,b,*]

[a] Department of Renewable Energy Engineering, University of Science and Technology (UST), 217 Gajeong-ro, Yuseong-gu, Daejeon, 34113, South Korea
[b] Fuel Cell Laboratory, Korea Institute of Energy Research (KIER), 152 Gajeong-ro, Yuseong-gu, Daejeon, 34129, South Korea
[c] Energy Materials Research Center, Korea Research Institute of Chemical Technology, 141 Gajeong-ro, Yuseong-gu, Daejeon, 34114, South Korea

ARTICLE INFO

Keywords:
Hydrocarbon membrane
Durability
Fuel cells
Antioxidant
Cerium

ABSTRACT

A poly(p-phenylene)-based multiblock polymer is developed with an oligomeric chain extender and cerium (CE-sPP-PPES + Ce^{3+}) to realize better performance and durability in proton exchange membrane fuel cells. The membrane performance is evaluated in single cells at 80 °C and at 100% and 50% relative humidity (RH). The accelerated stability test is conducted 90 °C and 30% RH, during which linear sweep voltammetry and hydrogen permeation detection are monitored periodically. Results demonstrate that the proton conductivity of the pristine hydrocarbon membranes is superior to that of PFSA membranes, and the hydrogen crossover is significantly lower. In addition, a composite membrane containing cerium performs similarly to a pristine membrane, particularly at low RH levels. Adding cerium to CE-sPP-PPES + Ce^{3+} membranes improves their chemical durability significantly, with an open circuit voltage decay rate of only 89 μV/h for 1000 h. The hydrogen crossover is maintained across accelerated stability tests, as confirmed by hydrogen detection and crossover current density. The short-circuit resistance indicates that membrane thinning is less likely to occur. Collectively, these results demonstrate that a hydrocarbon membrane with cerium is a potential alternative for fuel cell applications.

1. Introduction

Fuel cells that utilize polymer electrolyte membranes (PEMFC) are a promising alternative for converting energy. This technology can convert energy from hydrogen gas into electricity at approximately 60% efficiency, which is realized by not following the Carnot cycle [1]. The electrochemical performance of this method is highly dependent on the activation loss of the catalyst, the ohmic loss of the cell, and the loss in the reactant supply [2]. State-of-the-art PEMFCs adopt an ultra-thin membrane (less than 15 μm) to reduce the cell's ohmic loss, which eventually governs the overall performance of the fuel cell [3]. However, the durability of the thin membrane is a critical factor in terms of effective commercialization of PEMFCs [4]. In addition, the demand for durable membranes is increasing in PEM water electrolyzers (WE) because clean hydrogen generation and renewable energy are required.

A high-performance membrane is distinguished by its high proton conductivity and durability, both mechanically and chemically

* Corresponding author. Fuel Cell Laboratory, Korea Institute of Energy Research, 152 Gajeong-ro, Daejeon, 34129, South Korea.
E-mail address: bcbae@kier.re.kr (B. Bae).

https://doi.org/10.1016/j.heliyon.2024.e26680
Received 28 October 2023; Received in revised form 27 January 2024; Accepted 17 February 2024
Available online 19 February 2024

[5]. For example, perfluorosulfonic acid (PFSA) has been the benchmark membrane used in PEMFCs and WEs due to its excellent properties; however, PFSA loses its mechanical integrity and proton conductivity at temperatures above 100 °C due to its lower glass-transition temperature (Tg) and the boiling point of water [6]. In addition, the high cost of PFSA due to the perfluorinated nature in the polymer backbone limits its practical applicability [7]. Recent environmental regulations implemented by the United States (USA) and European governments suppress fluorine chemistry. As a result, sulfonated hydrocarbon-based membranes have emerged as a competitive alternative to PFSA membranes because they offer improved durability and incur lower costs for FCs and WEs.

Generally, hydrocarbon-based membranes comprise an aliphatic or aromatic benzene ring with a C–C and C═C bond linked as a backbone. The primary backbone of the sulfonated membranes is poly(ether sulfone) (PES), polysulfone (PSF), poly(aryl ether ketone) (PAEK), polybenzimidazole (PBI), and polyimides (PI) [8]. Although PFSA currently outperforms these membranes, recent studies have demonstrated significant improvements in their proton conductivity and durability, thereby making them practical alternatives. For example, several recent studies have reported proton conductivities approaching or exceeding those of PFSA, which demonstrates the potential of hydrocarbon-based membranes as a suitable replacement for PFSA [9,10].

Chemical durability is another critical issue for hydrocarbon membranes. For example, sulfonated poly(arylene ether sulfone)s (SPES) membranes have been reported to lose the sulfonic acid group when it is in an ortho position to the ether linkage [11]. The heterocycle atoms, e.g., sulfone and ketone, are susceptible to chemical degradation even though aromatic polymers require those linkages to increase solubility. An SPES membrane can degrade due to the scission of sulfone bridges [12], and, according to Shimizu et al. the removal of ketone groups in the hydrophilic structure can suppress the chemical decomposition of sulfonated phenylene poly (arylene ether ketone) [13]. Hydrolytic degradation of PI is a primary factor in their degradation [14].

Among hydrocarbon membranes, sulfonated polyphenylene receives more attention due to its superior chemical stability compared to poly arylene ethers or their derivatives. The aryl-aryl bond composing the backbone has dissociation energy at 479 ± 6 kJ/mol for biphenyl (C_6H_5–C_6H_5) is ~35% higher than that of diphenyl ether (C_6H_5O–C_6H_5 = 355 ± 6 kJ/mol) [15], which makes it more stable to decompositions. However, polyphenylene also requires heterocycle linkage to increase its solubility to serve as a membrane; thus, electron-rich ether groups next to the phenyl ring can be sweet spots for radical attacks [16,17]. In addition, pendant phenyl rings are then oxidized to carboxylic acid, which causes polymer degradations via ring-opening [17]. Therefore, the chemical stability of polyphenylene must be improved to compete with PFSA, e.g., by modifying its chemical structure or adding external chemical stabilizers.

One method to achieve this involves introducing radical scavengers or antioxidants into the polymer membrane, e.g., a transition metal [18,19], organic-metal complex [20], and organic and polymeric molecules [21]. Organic-type antioxidants have been utilized previously to improve the durability of polymer electrolyte membranes, e.g., terephthalic acid [22], 3,4-dihydroxycinnamic acid [23], and α-tocopherol [24]. Including 2,2′-bipyridine and 2,6-dimethoxy-1,4-benzoquinone in SPES-50 membranes can effectively double the lifetime compared to the pristine one [25]. The more extensive version of the organic-type, i.e., macromolecular antioxidants, are also effective [26]; however, the most effective antioxidants to date are Ce^{3+} metal ions. If they were once oxidized by OH• radicals, they can be active again after reduction by H_2O_2. Shin et al. incorporated Ce^{3+} metal ions into an SPES membrane, and the durability was improved five times compared to reference [27].

Based on the background mentioned above, an oligomeric chain extender-derived poly(p-phenylene)-based multiblock (CE-sPP-PPES, Fig. 1) membrane was synthesized and its PEMWE performance was reported in a previous study [28]. This membrane appears to be an effective alternative candidate for PFSA; thus, we modified the membrane with Ce^{3+} metal ions antioxidants to realize enhanced oxidative durability in PEMFC applications. Several investigations have addressed hydrocarbon membranes incorporating cerium; however, most studies have primarily focused on characterizing electrolyte membranes. Our present study comprehensively assessed the Membrane Electrode Assembly (MEA) performance and Open Circuit Voltage (OCV) durability of hydrocarbon membrane with cerium. Our objective is to provide a detailed analysis of the potential impacts of cerium ions during the practical operation of MEAs. This approach allows us to extend beyond mere membrane characterization and delve into the nuanced evaluation of overall MEA performance and the longevity of OCV under the influence of cerium-containing hydrocarbon membrane.

The CE-sPP-PPES + Ce^{3+} composite membranes were tested in single cells at 80 °C and 100% and 50% relative humidity (RH) for performance tests. In addition, the membrane was exposed to the OCV accelerated stability test suggested by the Department of Energy (USA) protocol. During durability tests, the properties of the membrane-electrode electrode assembly (MEA) were monitored via

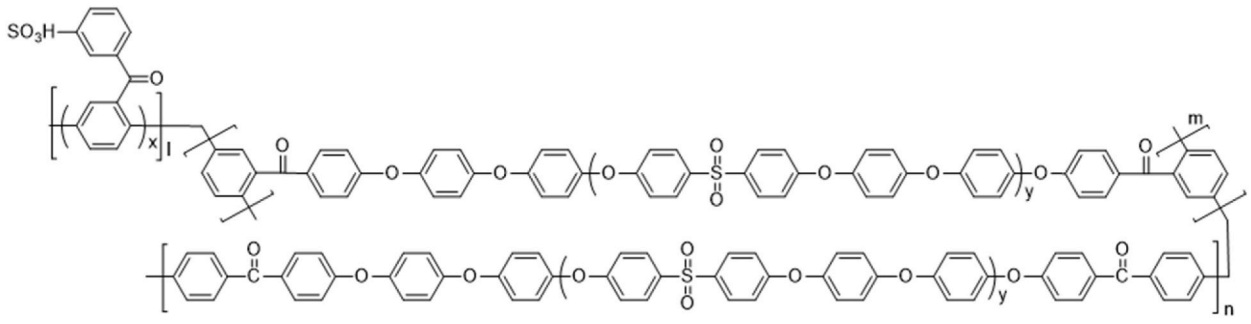

Fig. 1. Chemical structure of CE-sPP-PPES membrane [28].

hydrogen permeation detection, and linear sweep voltammetry (LSV). We report that the CE-sPP-PPES + Ce^{3+} membranes outperformed NR 211 in terms of the initial fuel cell performance and long-term stability.

2. Experimental conditions

2.1. Materials

N, N-Dimethylacetamide (DMAc, STBK7012), Bis(4-chlorophenyl) sulfone (BCPS, STBJ8128, Merck), 4,4′-dihydroxydiphenyl ether (DHDPE, STBJ3296), toluene (SHBB4678V), triphenylphosphine (TPP, WXBC9640V), nickel(II) bromide ($NiBr_2$, MKCC9410), zinc (STBK1875), cerium nitrate hexahydrate, and Aquivion dispersion D72-25BS (MKCG4230) were purchased from Sigma-Aldrich (Merck). Nafion NR 211 membranes (thickness ~25 μm) were purchased from DuPont, USA, and used as received without modification. Potassium carbonate (K_2CO_3, 062321) was purchased from Samchun, South Korea. The electrocatalysts TEC10F50E (1016–5731) and TEC61E54 (613–1411) were purchased from Tanaka, Japan and *N*-Methyl-2-pyrrolidone (NMP, IBS111) and hydrochloric acid (HCl, LC2112) were purchased from Duksan Pure Chemicals, South Korea. In this study, 4-Chloro-4′-fluorobenzhophenone (CFBP), 2,5-dichloro-4′-fluorobenzhophenone (FDCBP), and 2,5- dichloro-3′-sulfobenzhophenone (SDCBP) were synthesized following the process described in the literature [29].

2.2. Synthesis of polymers

Hydrophobic oligomers with three different terminations were synthesized according to the literature [28]. To prepare an OH-terminated oligomer, the DMAc solution containing K_2CO_3, BCPS, and DHDPE was mixed with toluene in a round bottom flask at 160 °C. Then, the toluene was removed through the Dean–Stark trap after 3 h. Heating continued at 165 °C for 16 h followed by removal of K_2CO_3. The mixture was then poured into methanol to obtain the products. Here, the OH-terminated oligomer was purified by washing it with hot methanol and hot water, and then drying overnight in a vacuum oven. The chlorobenzophenone (CBP)- and dichlorobenzophenone (DCBP)-terminated oligomers were synthesized in a similar manner, except the reaction occurred at 130 °C for 16 h and 150 °C for 2 h, respectively. Note that both oligomers contain an OH-terminated oligomer as a precursor with CFBP and FDCBP for the former and latter, respectively.

For polymer synthesis, a catalyst comprising $NiBr_2$, TPP, and zinc was mixed with anhydrous DMAc in a reaction flask equipped with an oil bath under an inert atmosphere at 80 °C with stirring. The anhydrous DMAc solutions containing SDCBP-, CBP- and DCBP-terminated oligomers were injected into the catalyst solutions after the color changed from light brown to reddish-brown. After 15 h of polymerization at 80 °C, the solution was precipitated in an ethanol and 10% HCl solution. The CE-sPP-PPES polymer with 2.0 meq/g ion exchange capacity (IEC) was purified by washing with hot ethanol and hot water, and then dried in a vacuum oven at 80 °C.

2.3. Membrane preparation

The electrolyte membrane was fabricated using the solution casting method. Cerium nitrate which was calculated based on sulfonated group on polymer were dissolved in 5 mL of DMSO, The CE-sPP-PPES polymer was dissolved in NMP, and 2.5 mol% Ce^{3+} Solution (relative to IEC) was added for the composite counterpart (CE-sPP-PPES + Ce^{3+}). The solution was then filtered using a syringe filter with a 5-μm PTFE filter membrane, cast on a clean glass plate using a casting accessory, and dried at 70 °C for 8 h. The dried membrane was then peeled by immersion in deionized water. Finally, the membrane was immersed in a 1.5 M H_2SO_4 aqueous solution at room temperature for 24 h to change the membrane to proton form. Here, the film thickness was controlled to 42 or 15 μm.

2.4. Membrane-electrode assembly preparation

The pristine sulfonated poly(p-phenylene)–based multiblock polymer with oligomeric chain extender (CE-sPP-PPES) membranes (thickness: ~15 μm) was used as a control with the NR 211 membranes. The MEA was prepared by laminating the membrane with an electrode using the decal transfer method. The PFSA ionomers were sprayed onto the surface of the membrane to realize better decal transfer for the hydrocarbon membrane. The electrodes were made of Aquivion D72 and carbon-supported PtRu electrocatalyst (TEC61E54) for the anode and carbon-supported Pt electrocatalyst (TEC10F50E) for the cathode. The PtRu electrocatalyst was selected because it has a greater tolerance to CO_2 than Pt. CO_2, an impurity in H_2 gas, can catalytically transform into CO and poison the catalyst surface, thereby reducing the performance [30,31]. The membrane-electrode sandwich was hot-pressed at 120 °C and 30 bar for 20 min, resulting in a catalyst loading of approximately 0.25 mgPtRu/cm^2 at the anode and 0.25 mgPt/cm^2 at the cathode. Then, the MEAs were assembled into single cells (InWooTech, South Korea) with a graphite bipolar plate, which provided a 25 cm^2 active area and a gas diffusion layer of 10 BC (SGL Carbon, Germany; 420 μm thickness, one side Microporous Layer (MPL), hydrophobized substrate (5 wt% PTFE), no hydrophobic coating). The single cell was pressed at 5.5 kgf/cm^2 and then connected to a temperature and humidity controller.

2.5. Fuel cell performance tests

We tested the fuel cell performance of the MEA at 80 °C, 100% and 50% RH using a Biologic HCP 803 potentiostat (BioLogic, France). Conditions for performance test and the following test is summarized in Table 1. Prior to conducting this test, the MEA was

activated overnight by holding the voltage at 0.8 V, 0.4 V, and 0.6 V to increase the kinetics of the charges in the electrode. The performance test began by withdrawing current from the cells as voltage scanned from OCV to 0.3 V and reversely with a 5 mV/s scan rate. The scanning process was performed 10 times, and LSV was measured to obtain the gas crossover of the membrane. This procedure is described in detail in Section 2.7.

2.6. Oxidative accelerated stability test

The condition of Accelerated Stability Test (AST) and in-situ analysis is shown in Table 1. Here, the OCV of MEA was recorded under 200 sccm H_2 and 420 sccm air at 90 °C and 30% RH. The MEA properties were monitored every 100 h by measuring the hydrogen permeation (HP) and LSV. The amount of 200 sccm H_2 gas permeating through the membrane was detected using the Fast Thermal Conductivity Analyzer FTC300 (Messkonzept GmbH, Germany) under 1000 sccm N_2. The HP unit was converted from ppm to Barrer to remove the thickness effect as follows [32]:

$$P = \frac{q \times t}{A \times \Delta p} \tag{1}$$

Here, P is the permeability (Barrer), q is the mass flux of gas through a membrane (cm^3(STP).sec^{-1}), which can be derived by converting flux in ppm (1 ppm $= \frac{1}{10^6}$L.min^{-1} $= \frac{1}{10^6} \times \frac{10^3}{60}$ cm^3 .sec^{-1}) of area A (cm^2) and thickness t (μm), under a partial pressure gradient Δp (cmHg or atm) across the membrane.

2.7. Electrochemical characterization

The electrochemical properties were measured using the BioLogic HCP 803 potentiostat/galvanostat.

2.7.1. Linear sweep voltammetry

LSV was conducted after the voltage of MEA was stable below 0.2 V; however, the N_2 continued to flow in the cathode during measurement. At a rate of 1.0 mV/s, the voltage scanned from 0.1 to 0.6 V to withdraw the gas crossover current. Extrapolation of the data line from 0.4 V to 0.5 V serves two pieces of information. The y-axis offset signifies the crossover current density/$j_{crossover}$ (mA/cm^2), determined by hydrogen permeation through the membrane. The inverse of the gradient reflects the short-circuit resistance/R_{sc} (mΩ.cm^2), indicating the membrane's electron transport capability. Lower R_{sc} values suggest direct electron passage, indicating membrane thinning. These properties can be utilized to determine the status of the membrane.

2.7.2. Electrochemical impedance spectroscopy

The potentiostatic EIS was measured by scanning a 0.2 V potential difference with a frequency from 50 kHz to 5 Hz under 200 sccm H_2 and 1000 sccm N_2. From the Nyquist plot, the interception of the curve to the x-axis indicates high-frequency resistance (HFR).

3. Results and discussion

3.1. Fuel cell performance of CE-sPP-PPES membranes

3.1.1. Performance of pristine CE-sPP-PPES membrane

In our previous study [28], we found that the CE-sPP-PPES membrane performed better than Nafion 115 in the PEMWE. Unlike WE, which uses preheated liquid water [33], FC only uses humidified gas to feed into the MEA. Partial humidification will avoid excessive swelling in the MEA or membrane, which will result in premature dimensional stability issues and performance decay [34]. Fig. 2 shows the performance curve of the pristine CE-sPP-PPES membranes compared to the Nafion NR 211 membrane at 80 °C and 100% and 50% RH. The CE-sPP-PPES (15 μm) membrane demonstrated better performance than Nafion NR 211. As shown in Table 2, the current density at 0.6 V (j @ 0.6 V) is 1337 mA/cm^2 for the former, which is higher than the 1039 mA/cm^2 result for the latter. In addition, the thicker CE-sPP-PPES (42 μm) exhibits the lowest performance, i.e., 454 mA/cm^2. A similar trend is also exhibited by the *HFR* data in the lower part of Fig. 2 and in Table 2, which confirms the consistency of the results. However, considering the difference

Table 1
Conditions of the performance, accelerated stability tests (ASTs) and *in situ* analyses.

Step	Gas Flow (NmL/min)		Temperature (°C)	Relative Humidity (%)	Gas Pressure (Pa)
	Anode	Cathode			
Activation	H_2 350	Air 1500	80	100	Ambient (1.01×10^5)
Performance				100 & 50	
Electrochemical Impedance Spectroscopy	H_2 200	N_2 1000			
Linear Sweep Voltammetry	H_2 200	N_2 1000			
AST	H_2 200	Air 420	90	30	
Hydrogen permeation	H_2 200	N_2 1000			
Linear Sweep Voltammetry	H_2 200	N_2 1000			

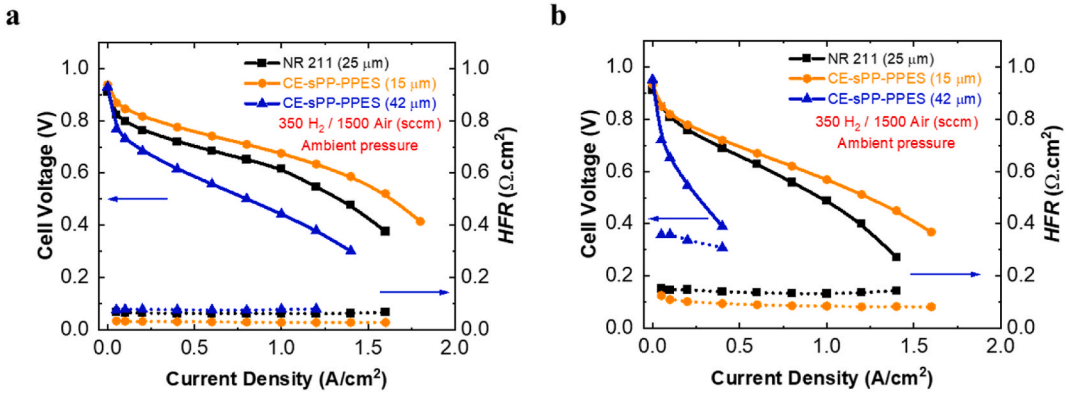

Fig. 2. Fuel cell performance (upper) and ohmic resistance (lower) of pristine CE-sPP-PPES membranes at 80 °C and (a) 100% and (b) 50% RH.

in membrane thickness and cell performance, these results do not appear straightforward. Thus, it is necessary to utilize the through-plane conductivity parameter to compensate for the thickness, which is derived by converting the area resistance *HFR* (mΩ.cm^2) into conductivity σ (S/m) as follows [35].

$$\sigma = \frac{l}{R \times A} = \frac{l}{HFR}, \tag{2}$$

where l (μm) and A (cm^2) are the thickness and area of the membrane, respectively. Additional details about the conversion are shown in Table S1, and the results are plotted in Fig. 3.

The *in situ* through-plane conductivity of NR 211 from this experiment is approximately 0.041 S/cm (at 1000 mA/cm^2), which differs from previously reported results because it is highly dependent on the membrane history and measurement conditions [36]. For example, Soboleva et al. reported that the *ex situ* through-plane conductivity of Nafion NR 211 is 0.059 S/cm, which is similar to the in-plane conductivity due to the isotropy of NR 211 [37]. However, in-plane conductivity measurements conducted by the same group using the same setup, but performed by Peron et al. yielded a higher value of 0.13 S/cm [38], representing a discrepancy of greater than 50%. In the former case, the membranes were soaked in DI water for 24 h, and the impedance data were recorded in water. In the latter case, the impedance data were humidity-dependent, and the membranes were equilibrated for 2 h under vapor exposure. These differences have a significant impact on conductivity measurements. In addition, Slade et al. noted a substantial variation in the conductivity of Nafion 117 measured by different research groups [36]. Thus, it is not surprising that the conductivity of NR 211 observed in the current study differs from previous findings. Note that the membrane used in this experiment was utilized as received without modification, and the decal transfer process involved hot-pressing, which can alter the morphologies and surface properties of NR 211, thereby inducing non-negligible reduction of the through-plane conductivity [39,40].

From the results shown in Table S1 and Fig. 3, it is obvious that CE-sPP-PPES membranes have higher through-plane conductivity than Nafion NR 211, i.e., up to 40% higher, which validates its superiority compared with PFSA. As confirmed by a previous report [28], the multiblock structure of this poly(p-phenylene)-based copolymer with 2.0 meq/g exhibited better proton conductivity in the fully swollen condition. In the previous study, transmission electron microscopy images suggested the microphase-separated morphology of the CE-sPP-PPES membranes [28]. However, it is still not as strong as the phase separation of Nafion, as demonstrated by the SAXS data from the same report. The higher IEC of the hydrocarbon membrane appears to significantly compensate for the abovementioned disadvantages in terms of better membrane performance.

In Fig. 3 (a), unlike NR 211 and the thicker CE-sPP-PPES (42 μm), the thinner CE-sPP-PPES (15 μm) membrane exhibits a variation in its conductivity according to the current density. For example, at 50 mA/cm^2, the 15-μm membrane exhibits 0.045 S/cm in its

Table 2
Properties of MEA during fuel cells performance test.

Membranes	OCV	j @ 0.6 V	Tafel slope	*HFR* @ 50 mA/cm^2	*HFR* @ 1000 mA/cm^2	$j_{crossover}$	R_{sc}
	(V)	(mA/cm^2)	(mV/dec)	(mΩ.cm^2)	(mΩ.cm^2)	(mA/cm^2)	(mΩ.cm^2)
80 °C 100% RH							
NR 211 (25 μm)	0.909	1039	−52	66	62	1.25	729
CE-sPP-PPES (15 μm)	0.937	1337	−43	33	28	0.13	633
CE-sPP-PPES (42 μm)	0.928	454	−94	77	78	0.11	3571
80 °C 50% RH							
NR 211 (25 μm)	0.910	680	−56	151	132	1.37	315
CE-sPP-PPES (15 μm)	0.933	878	−49	125	85	0.45	1666
CE-sPP-PPES (42 μm)	0.951	139	−129	358	–	0.01	4545

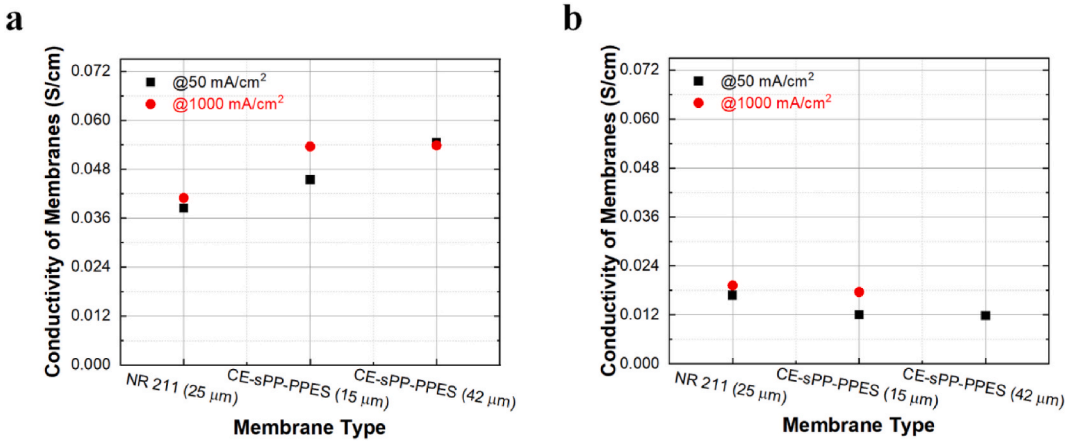

Fig. 3. Conductivity of CE-sPP-PPES versus NR 211 membrane at 80 °C and (a) 100%, and (b) 50% RH.

conductivity, whereas it shows 0.054 S/m at 1000 mA/cm^2. Note that a very similar trend is observed under the 50% RH condition, although the 45-μm membrane does not appear to be sensitive to current density. Such variation may be due to the higher water diffusion of water from the cathode and osmotic drag to the cathode [41,42]. That water balance is complicated to predict exact water uptake of the membrane in the operating cell; thus, we estimate that the thinner membrane is more sensitive to water balance due to its thickness. A possible postulation is that the 15-μm membrane exhibits a lower ion conductivity at 50 mA/cm^2 than at 1000 mA/cm^2 when exposed to 100% and 50% RH. This behavior is attributed to the greater back diffusion of water from the cathode of the MEA, where, at higher current densities, the diffusion of water moving due to back diffusion can exceed the water flow driven by the osmotic drag. Consequently, a higher ion conductivity value is observed at high current densities. Note that similar behavior has been reported in the literature [36,43], where the HFR of the MEA is a function of membrane thickness and current density. Nevertheless, we can conclude that CE-sPP-PPES outperformed the Nafion membrane in terms of conductivity under the 100% RH condition, which is in good agreement with the results of the *ex situ* conductivity test.

However, the Tafel slope differs among those MEAs. As shown in Table 2 and Fig. S1, CE-sPP-PPES (15 μm) exhibits the lowest Tafel slope, i.e., −43 mV/dec, followed by Nafion NR 211 and CE-sPP-PPES (42 μm) at −52 mV/dec and −94 mV/dec, respectively. This trend is somewhat similar to *j* @ 0.6 V and *HFR*. Even though identical electrodes were used, their properties could differ, possibly due to the difference in how the ionomer developed during activation. According to Christmann et al. the amount of water in the MEA can accelerate activation [44]. Even though the proton conductivity of the bulk membrane plays a subordinate role in the activation, water diffusion can affect catalyst activity during the break-in of the MEA [45]. Data in Table S2 support this idea where catalytic mass activity of CE-sPP-PPES (15 μm) is significantly higher than that of other MEAs despite comparable ECSA. It can also naturally restructure the ionomer to reorganize itself toward a relaxed state [46]. Thus, a thinner membrane MEA could have a lower Tafel slope, as shown in Table 2.

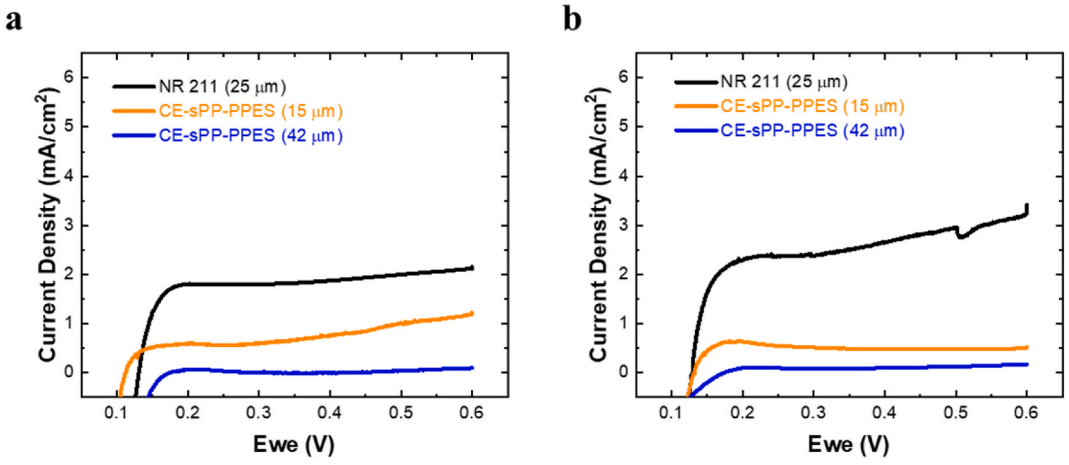

Fig. 4. LSV of pristine CE-sPP-PPES vs NR 211 membrane at 80 °C and (a) 100% RH and (b) 50% RH.

3.1.2. Membrane's hydrogen permeation

The LSV quantifies two parameters, i.e., the crossover current density, which represents the amount of gas/hydrogen crossover through the membrane, and the short-circuit resistance, which explains how effectively the membrane blocks the electron from moving from one electrode to the other, typically depending on the membrane's thickness [47]. The LSV curve from the pristine CE-sPP-PPES membrane is shown in Fig. 4. The CE-sPP-PPES curve is located below 1 mA/cm^2 and is clearly in a lower position than the Nafion NR 211 membrane, approximately 2 mA/cm^2. Generally, the CE-sPP-PPES membrane has lower gas permeation than the NR 211 membrane. The crossover current density ($j_{crossover}$) and short-circuit resistance (R_{sc}) values are shown in Table 2. As can be seen, the CE-sPP-PPES membrane has lower $j_{crossover}$ at 0.13 mA/cm^2 and 0.11 mA/cm^2 for thicknesses of 15 μm and 42 μm, respectively, which is lower than the NR 211 membrane at 1.25 mA/cm^2. Consequently, the OCV of the CE-sPP-PPES membrane is higher than that of Nafion, i.e., 0.937 V (at 15 μm) and 0.928 V (at 42 μm) vs. 0.909 V (Nafion), respectively.

Naturally, the hydrocarbon membrane has a lower gas crossover than PFSA due to the polymer molecule structure made of a phenyl ring (benzene) and its high glass-transition temperature [48]. This structure enables polymer molecules to become stacked so closely and tightly that a small amount of free volume is left for gas to permeate the membrane [49]. In contrast, Nafion has a PTFE backbone and a long side chain in its polymer structure, which allows more free volume and low glass-transition temperature [50]. In addition to its superior proton conductivity, the CE-sPP-PPES membrane exhibits lower gas permeation, thereby making it even more valuable in fuel cells.

3.1.3. Cerium effect on membrane performance

Incorporating cerium is meant to increase membrane durability; thus, its effect on the membrane or MEA performance is expected to be nonexistent or negligible. The fuel cell performance of the composite CE-sPP-PPES + Ce^{3+} membranes is shown in Fig. 5, and the detailed information is given in Table 3. The I–V curve of the composite CE-sPP-PPES + Ce^{3+} membranes overlaps that of the pristine one in the low-mid current density, which indicates that the performance of the catalyst (low region) of both MEAs is similar. The graph of the Tafel slope in Fig. S2 and the details given Table 3 further confirm that the Tafel slope of the composite CE-sPP-PPES + Ce^{3+} (15 μm) is comparable to that of the pristine one. These results demonstrate that the presence of cerium in the membrane does not affect catalyst performance.

As shown in Fig. 5, the performance of the composite CE-sPP-PPES + Ce^{3+} membrane is slightly lower than that of the pristine membrane. Despite having the same thickness as the pristine membrane, the composite membrane shows lower I–V performance under high current density.

The current density at 0.6 V (j @ 0.6 V) of the composite membrane is 1011 mA/cm^2 and 767 mA/cm^2 at high and low RH, respectively, which is lower than that of the pristine counterpart (Table 3). For better analysis, the *HFR* at 50 and 1000 mA/cm^2 is converted to through-plane conductivity to be the same as the pristine membranes, as shown in Table S2 and Fig. 6. The composite CE-sPP-PPES + Ce^{3+} membrane exhibits lower conductivity than the pristine membrane, even though it has the same thickness. Some researchers have reported that cerium induces crosslinking among sulfonic groups to suppress its proton conduction [51]. We also observed a similar phenomenon [27,52], where the through-plane ion conductivity of the electrolyte membrane containing cerium was low. Similarly, as shown in Fig. 6, the difference in conductivity according to current density observed in the cerium-free electrolyte membrane can be observed in the electrolyte membrane containing cerium. Perhaps, at high current densities, water movement appears to occur somewhat similarly regardless of the presence of cerium. Typically, current density increases correlate with increased water generation at the cathode. This phenomenon induces back diffusion, consequently elevating the ionic conductivity of the electrolyte membrane. Notably, our observations suggest that the back diffusion phenomenon manifests uniformly, irrespective of the presence or absence of cerium. This implies that the influence of current density on water generation and subsequent back diffusion remains consistent, emphasizing the inherent behavior of the system, irrespective of cerium's presence.

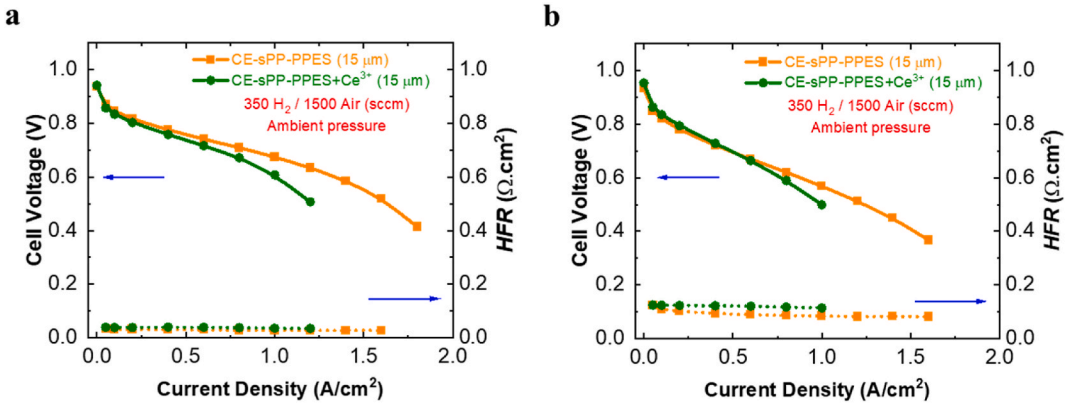

Fig. 5. Fuel cell performance (upper) and ohmic resistance (lower) of composite CE-sPP-PPES + Ce^{3+} membranes at 80 °C and (a) 100% and (b) 50% RH.

Table 3
Properties of composite CE-sPP-PPES + Ce^{3+} membrane-based MEAs during performance tests.

Membranes	OCV	*j* @ 0.6 V	Tafel slope	*HFR* @ 50 mA/cm^2	*HFR* @ 1000 mA/cm^2
	(V)	(mA/cm^2)	(mV/dec)	(mΩ.cm^2)	(mΩ.cm^2)
80 °C 100% RH					
CE-sPP-PPES (15 μm)	0.937	1337	−43	33	28
CE-sPP-PPES + Ce^{3+} (15 μm)	0.942	1011	−51	40	36
80 °C 50% RH					
CE-sPP-PPES (15 μm)	0.933	878	−49	125	85
CE-sPP-PPES + Ce^{3+} (15 μm)	0.953	767	−52	125	115

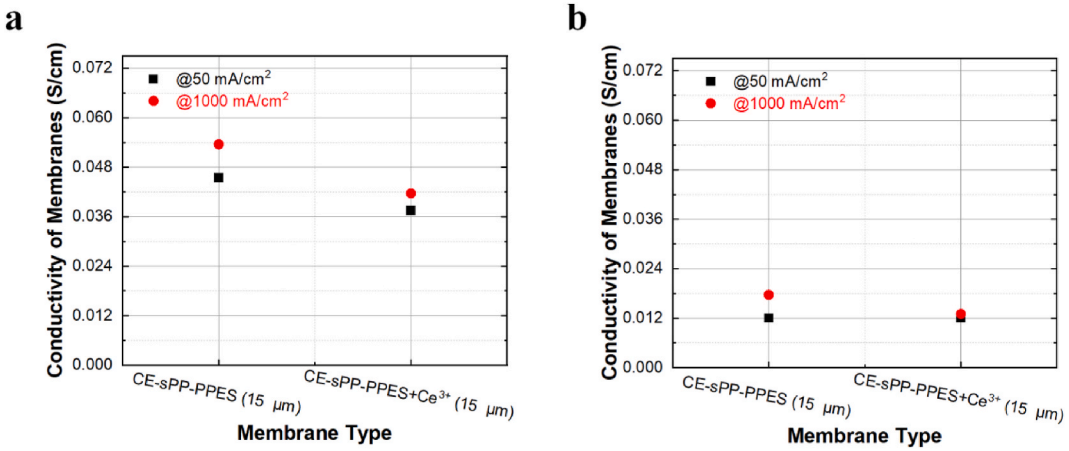

Fig. 6. Conductivity of composite CE-sPP-PPES + Ce^{3+} membranes at 80 °C and (a) 100% RH and (b) 50% RH.

3.2. Accelerated stability test of CE-sPP-PPES+Ce^{3+} membranes

3.2.1. Effect of cerium on CE-sPP-PPES + Ce^{3+} membranes durability

OCV is used to indicate the membrane status (i.e., the oxidative durability) because it is susceptible to the amount of crossover gas through the membrane. The potential difference between the cathode and anode is maximum when no or fewer gases permeate the membrane. When gas permeation occurs due to a damaged membrane, e.g., gases mix at either electrode, thereby causing mixed potential, the OCV is reduced. The initial OCV of fresh MEA, which is related to the initial gas permeation, indicates the inherent property of the membrane. Fig. 7a and Table S3 show that the initial OCV of the pristine and composite CE-sPP-PPES + Ce^{3+} membranes are very similar (approximately 0.98 V), which indicates that their inherent properties in terms of gas permeation are

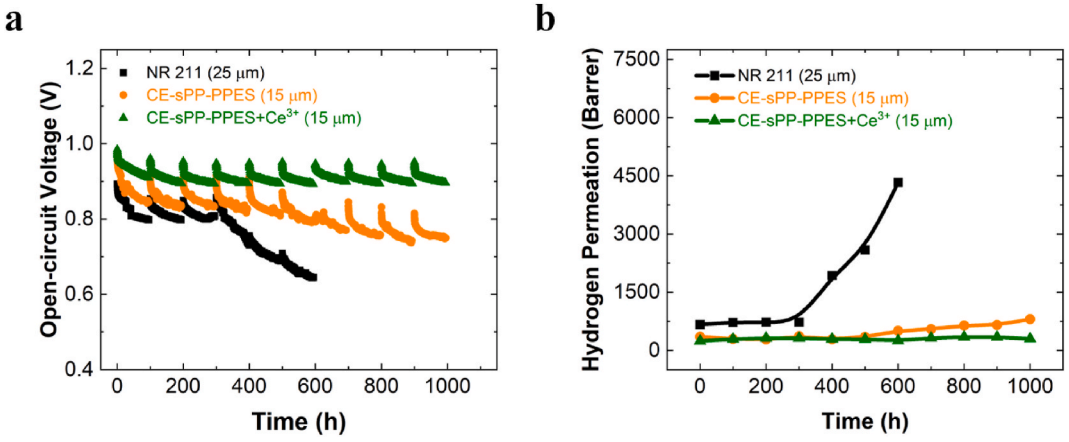

Fig. 7. (a) Open-circuit voltage and (b) hydrogen permeation of composite CE-sPP-PPES + Ce^{3+} versus pristine counterpart and NR 211 membranes during AST at 90 °C and 30% RH.

comparable. However, the NR 211 membrane has a much lower initial OCV at 0.89 V due to its higher gas permeation, which is confirmed in Fig. 7b. The effect of cerium on the long-term durability of CE-sPP-PPES membranes is shown in Fig. 7a. As can be seen, the composite CE-sPP-PPES + Ce^{3+} maintains OCV for 1000 h of AST. With only 89 μV/h of average OCV decay rate, as shown in Table S3, the CE-sPP-PPES + Ce^{3+} (15 μm) membranes lasted at 0.90 V in the final OCV. In addition, the pristine CE-sPP-PPES membranes finish at 0.75 V with 222 μV/h of average OCV decay rate, representing approximate three times faster degradation rate than the composite membrane. This result elucidates that cerium effectively scavenges free radicals that boost CE-sPP-PPES membranes' durability. It is even better when compared to the NR 211 membrane, which only lasts 600 h at 0.64 V with a much higher average OCV decay rate (414 μV/h). These results reveal that pristine CE-sPP-PPES membranes are much more durable than NR 211 membranes, and adding cerium enhances the durability to an even higher level.

Numerous previous studies have discussed how cerium effectively increases membrane durability. For example, Endoh [51] philosophically elaborated that the cerium cation can reduce hydroxyl radicals into water molecules and regenerate to the original ionic state after oxidation by H_2O_2 [51], which is what makes cerium active continuously. In addition, Gubler et al. [53] supported this concept theoretically. However, in hydrocarbon membranes, the rate constant for HO• radicals to attack the aromatic units is in the order 10^9–10^{10} $M^{-1}s^{-1}$, which is much faster than that of the scavenging reaction with cerium, i.e., 3.10^8 $M^{-1}s^{-1}$ [54]. As a result, the half-life of free radicals is relatively too short, i.e., approximately 20 ns, compared to microseconds in PFSA, which is insufficient to scavenge a considerable amount of HO• radicals. Radical scavenging by cerium is supposedly less effective in hydrocarbon membranes than in PFSA [55]. In contrast, the findings of the current study demonstrate that cerium has an excellent effect on the durability of hydrocarbon membranes. Experimental studies performed by other groups have shown similar results [52,56,57].

3.2.2. *In situ analysis during OCV holding test*

3.2.2.1. Hydrogen permeation. The HP of the composite CE-sPP-PPES + Ce^{3+} membranes is shown in Fig. 7b. Initially (i.e., at 0 h), the pristine and composite hydrocarbon membranes have relatively low HP at beginning of the OCV test, <350 Barrer, which is half of that of the NR 211 membrane (700 Barrer). Note that this exactly matches the LSV analysis in the initial MEA performance test. The pristine CE-sPP-PPES membrane shows relatively stable HP until 500 h, and it increases gradually for the duration of the test. In contrast, the NR 211 membrane increases abruptly after 300 h due to severe chemical degradation. The cerium enhances the chemical durability of the CE-sPP-PPES + Ce^{3+} membranes significantly. The composite CE-sPP-PPES + Ce^{3+} membranes exhibit very stable and comparable HP across the AST. In addition to less radical production, the presence of cerium in the composite membrane can suppress the existence of radicals [51]. In turn, the membrane becomes safe and can maintain HP. As mentioned in Section 3.2.1, these results match the OCV curve.

3.2.2.2. Linear sweep voltammetry. In addition to the HP, LSV results are included to observe the membrane's gas permeability during AST, as shown in Fig. S3. Analysis from LSV graphs provides crossover current density ($j_{crossover}$) and short-circuit resistance (R_{sc}), as shown in Fig. 8. In line with the HP and OCV data, the $j_{crossover}$ of the hydrocarbon membranes is comparable and stable during the AST, which suggests that they are chemically stable, and that the crossover current density is maintained. Unlike the hydrocarbon membranes, the NR 211 membrane's $j_{crossover}$ value increases significantly after 300 h, indicating severe membrane degradation. In addition, as shown in Fig. S3 (a), at 600 h, the LSV curve stopped at 0.3 V due to critical damage.

In addition, membrane degradation can be observed from the short-circuit resistance (R_{sc}) behavior [47] in the upper part of Fig. 8. The electrolyte membrane is supposed to transport only protons or become an electron barrier; thus, the electronic resistance of the membrane is expected to be as high as possible [2]. The pristine and composite CE-sPP-PPES membranes have higher R_{sc} than NR 211 across the AST despite having lower thickness, exhibiting results of 591 mΩ.cm^2, 909 mΩ.cm^2, and 17 mΩ.cm^2 at the end of the test, respectively. These results suggest better chemical stability in the pristine and composite CE-sPP-PPES membranes. Moreover, the combination of an increased $j_{crossover}$ and decreased R_{sc} makes the LSV of NR 211 lifted and tilted, as shown in Fig. S3(a).

4. Conclusion

Our research demonstrates that the superior performance of the CE-sPP-PPES membrane over Nafion NR 211 in fuel cell applications is a significant advancement in polymer electrolyte membrane technology. This membrane exhibits enhanced current density at 0.6 V and a reduced Tafel slope, indicative of improved proton transport and catalyst activity. Its through-plane conductivity, up to 40% higher than that of Nafion NR 211, further validates its superior performance characteristics. Additionally, the CE-sPP-PPES membrane shows lower gas crossover, higher open-circuit voltage (OCV), and better durability, making it a more effective and reliable alternative for fuel cell membranes. Incorporating cerium into the CE-sPP-PPES membrane presents a nuanced outcome; it does not significantly affect the catalyst performance but slightly decreases conductivity and overall cell performance at high current densities. However, this is counterbalanced by a significant increase in chemical durability. The composite CE-sPP-PPES + Ce3+ membrane's OCV comparison suggests it possesses enhanced chemical durability compared to the pristine and perfluorosulfonic acid (PFSA) membranes. This balance of high performance and durability underlines the potential of the CE-sPP-PPES + Ce3+ membrane as a pivotal material in fuel cell technology.

Our findings underscore the potential of the CE-sPP-PPES + Ce3+ membrane in advancing fuel cell technology, positioning it as a highly innovative alternative to traditional membrane materials. The study paves the way for further research and development efforts aimed at optimizing the performance of this membrane, particularly in high-current density applications, and exploring its integration

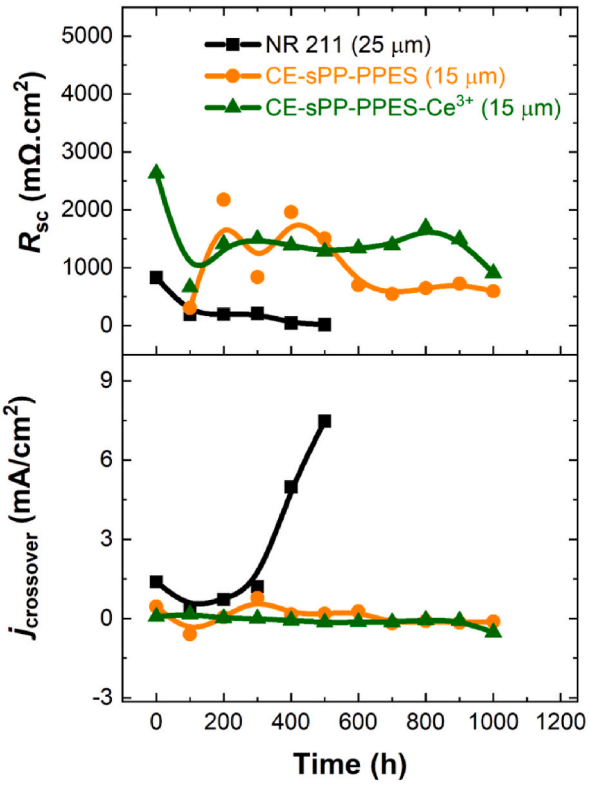

Fig. 8. Crossover current density (bottom) and short-circuit resistance (top) of pristine and composite CE-sPP-PPES + Ce^{3+} versus NR 211 membranes during AST at 90 °C and 30% RH.

into commercial fuel cell systems. This membrane's unique combination of performance characteristics and durability makes it a promising candidate for next-generation fuel cell applications, offering a pathway towards more efficient, durable, and cost-effective fuel cell technologies.

CRediT authorship contribution statement

Abdul Kodir: Writing – original draft. **Seunghee Woo:** Validation. **Sang-Hun Shin:** Investigation. **Soonyong So:** Investigation. **Duk Man Yu:** Investigation. **Hyejin Lee:** Supervision. **Dongwon Shin:** Supervision. **Jang Yong Lee:** Project administration. **Seok-Hee Park:** Project administration. **Byungchan Bae:** Writing – review & editing.

Declaration of Generative AI and AI-assisted technologies in the writing process

During the preparation of this work the authors did not use any generative AI tools.

Declaration of competing interest

The authors declare that they have no known competing financial interests or personal relationships that could have appeared to influence the work reported in this paper.

Acknowledgement

This work was supported by the framework of the Research and Development Program of the Korea Institute of Energy Research [C4-2406] and the Korea Institute of Energy Technology Evaluation and Planning grant [20203020030010] funded by the Korean government (MOTIE).

Appendix A. Supplementary data

Supplementary data to this article can be found online at https://doi.org/10.1016/j.heliyon.2024.e26680.

References

[1] Y. Luo, Y. Shi, N. Cai, Bridging a Bi-directional Connection between Electricity and Fuels in Hybrid Multienergy Systems, Elsevier, 2021, pp. 41–84.
[2] F. Barbir, PEM Fuel Cells: Theory and Practice, Elsevier Science, 2012.
[3] Y. Wang, D.F.R. Diaz, K.S. Chen, Z. Wang, X.C. Adroher, Materials, technological status, and fundamentals of PEM fuel cells–a review, Mater. Today 32 (2020) 178–203.
[4] N. Zamel, X. Li, Effect of contaminants on polymer electrolyte membrane fuel cells, Prog. Energy Combust. Sci. 37 (3) (2011) 292–329.
[5] K. Scott, 10 - Microbial fuel cells: transformation of wastes into clean energy, in: A. Gugliuzza, A. Basile (Eds.), Membranes for Clean and Renewable Power Applications, Woodhead Publishing, 2014, pp. 266–300.
[6] L. Merlo, A. Ghielmi, V. Arcella, Fuel cells – PROTON-EXCHANGE MEMBRANE FUEL CELLS | membranes: advanced fluorinated, in: J. Garche (Ed.), Encyclopedia of Electrochemical Power Sources, Elsevier, Amsterdam, 2009, pp. 680–699.
[7] G.H. Byun, J.A. Kim, N.Y. Kim, Y.S. Cho, C.R. Park, Molecular engineering of hydrocarbon membrane to substitute perfluorinated sulfonic acid membrane for proton exchange membrane fuel cell operation, Mater. Today Energy 17 (2020), https://doi.org/10.1016/j.mtener.2020.100483.
[8] R.R.R. Sulaiman, R. Walvekar, M. Khalid, W.W. Yin, P. Jagadish, Recent progress in the development of aromatic polymer-based proton exchange membranes for fuel cell applications, Polymers 12 (5) (May 6 2020) 1061, https://doi.org/10.3390/polym12051061 (Basel).
[9] F. Wijaya, S. Woo, H. Lee, A.F. Nugraha, D. Shin, B. Bae, Sulfonated poly(phenylene-co-arylene ether sulfone) multiblock membranes for application in high-performance fuel cells, J. Membr. Sci. 645 (2022) 120203, https://doi.org/10.1016/j.memsci.2021.120203, 03/05/2022.
[10] S.J. Hong, H.Y. Jung, S.J. Yoon, K.-H. Oh, S.-G. Oh, Y.T. Hong, D.M. Yu, S. So, Constrained hydrocarbon-based ionomers in porous Poly(tetrafluoroethylene) supports for enhanced durability of polymer electrolyte membrane fuel cells and water electrolyzers, J. Power Sources 551 (2022) 232221, https://doi.org/10.1016/j.jpowsour.2022.232221, 12/15/2022.
[11] B. Bae, K. Miyatake, M. Uchida, H. Uchida, Y. Sakiyama, T. Okanishi, M. Watanabe, Sulfonated poly(arylene ether sulfone ketone) multiblock copolymers with highly sulfonated blocks. Long-term fuel cell operation and post-test analyses, ACS Appl. Mater. Interfaces 3 (7) (2011) 2786–2793, https://doi.org/10.1021/am200579z.
[12] S. Takamuku, P. Jannasch, Properties and degradation of hydrocarbon fuel cell membranes: a comparative study of sulfonated poly(arylene ether sulfone)s with different positions of the acid groups, Polym. Chem. 3 (5) (2012-01-01 2012) 1202, https://doi.org/10.1039/c2py00611a.
[13] R. Shimizu, J. Tsuji, N. Sato, J. Takano, S. Itami, M. Kusakabe, K. Miyatake, A. Iiyama, M. Uchida, Durability and degradation analysis of hydrocarbon ionomer membranes in polymer electrolyte fuel cells accelerated stress evaluation, J. Power Sources 367 (2017) 63–71, https://doi.org/10.1016/j.jpowsour.2017.09.025.
[14] C. Genies, R. Mercier, B. Sillion, R. Petiaud, N. Cornet, G. Gebel, M. Pineri, Stability study of sulfonated phthalic and naphthalenic polyimide structures in aqueous medium, Polymer 42 (12) (2001) 5097–5105, https://doi.org/10.1016/s0032-3861(00)00645-5.
[15] Y.-R. Luo, Handbook of Bond Dissociation Energies in Organic Compounds, 2002.
[16] A. Kraytsberg, Y. Ein-Eli, Review of advanced materials for proton exchange membrane fuel cells, Energy Fuels 28 (12) (2014/12/18 2014) 7303–7330, https://doi.org/10.1021/ef501977k.
[17] T. Holmes, T.J.G. Skalski, M. Adamski, S. Holdcroft, Stability of hydrocarbon fuel cell membranes: reaction of hydroxyl radicals with sulfonated phenylated polyphenylenes, Chem. Mater. 31 (4) (2019) 1441–1449, https://doi.org/10.1021/acs.chemmater.8b05302.
[18] T. Bal-Demirci, M. Şahin, E. Kondakçı, M. Özyürek, B. Ülküseven, R. Apak, Synthesis and antioxidant activities of transition metal complexes based 3-hydroxysalicylaldehyde-S-methylthiosemicarbazone, Spectrochim. Acta Mol. Biomol. Spectrosc. 138 (2015) 866–872, https://doi.org/10.1016/j.saa.2014.10.088, 03/05/2015.
[19] S.J.S. Flora, Structural, chemical and biological aspects of antioxidants for strategies against metal and metalloid exposure, Oxid. Med. Cell. Longev. 2 (4) (2009) 191–206, https://doi.org/10.4161/oxim.2.4.9112, 01-01 2009.
[20] P.A. Khalaf-Alla, Antioxidant, antimicrobial and antitumor studies of transition metal complexes derived from N-(2-Aminoethyl)-1,3-Propanediamine with DFT calculations and molecular docking investigation, Appl. Organomet. Chem. 34 (5) (2020), https://doi.org/10.1002/aoc.5628, 05-01 2020.
[21] M. Naguib, M.A. Yassin, Polymeric antioxidant via ROMP of bioderived tricyclic oxanorbornene based on vanillin and furfurylamine, ACS Appl. Polym. Mater. 4 (3) (2022) 2181–2188, https://doi.org/10.1021/acsapm.2c00158, 03/11 2022.
[22] Y. Zhu, S. Pei, J. Tang, H. Li, L. Wang, W.Z. Yuan, Y. Zhang, Enhanced chemical durability of perfluorosulfonic acid membranes through incorporation of terephthalic acid as radical scavenger, J. Membr. Sci. 432 (2013) 66–72, https://doi.org/10.1016/j.memsci.2012.12.050.
[23] Y. Park, D. Kim, Chemical stability enhancement of Nafion membrane by impregnation of a novel organic ·OH radical scavenger, 3,4-dihydroxy-cinnamic acid, J. Membr. Sci. 566 (2018) 1–7, https://doi.org/10.1016/j.memsci.2018.08.063.
[24] Y. Yao, J. Liu, W. Liu, M. Zhao, B. Wu, J. Gu, Z. Zou, Vitamin E assisted polymer electrolyte fuel cells, Energy Environ. Sci. 7 (10) (2014) 3362–3370, https://doi.org/10.1039/c4ee01774a.
[25] S. Park, H. Lee, S.H. Shin, N. Kim, D. Shin, B. Bae, Increasing the durability of polymer electrolyte membranes using organic additives, ACS Omega 3 (9) (Sep 30 2018) 11262–11269, https://doi.org/10.1021/acsomega.8b01063.
[26] A. Kodir, S.H. Shin, S. Park, M.R. Arbi, T.H. Yang, H. Lee, D. Shin, B. Bae, Macromolecular antioxidants for chemically durable polymer electrolyte fuel cell membranes, Int. J. Energy Res. 46 (6) (2022) 7186–7200, https://doi.org/10.1002/er.7607.
[27] D. Shin, M. Han, Y.-G. Shul, H. Lee, B. Bae, Analysis of cerium-composite polymer-electrolyte membranes during and after accelerated oxidative-stability test, J. Power Sources 378 (2018) 468–474, https://doi.org/10.1016/j.jpowsour.2017.12.074. December 2017.
[28] S. Choi, S.-H. Shin, D.-H. Lee, G. Doo, D.W. Lee, J. Hyun, S.H. Yang, D. Man Yu, J.Y. Lee, H.-T. Kim, Oligomeric chain extender-derived poly(p-phenylene)-based multi-block polymer membranes for a wide operating current density range in polymer electrolyte membrane water electrolysis, J. Power Sources 526 (2022), https://doi.org/10.1016/j.jpowsour.2022.231146.
[29] J.Y. Lee, D.M. Yu, T.-H. Kim, S.J. Yoon, Y.T. Hong, Multi-block copolymers based on poly(p-phenylene)s with excellent durability and fuel cell performance, J. Membr. Sci. 492 (2015) 209–219, https://doi.org/10.1016/j.memsci.2015.04.013, 10/15/2015.
[30] Y. Okajima, A. Yamamoto, M. Sudoh, S. Sakai, Y. Matsumoto, Effect of carbon dioxide in hydrogen on PEMFC for using reformed gas from biogas, Electrochemistry 79 (5) (2011) 346–348, https://doi.org/10.5796/electrochemistry.79.346.
[31] Y. Feng, W. Han, T. Wang, Q. Chen, Y. Zhang, Y. Sun, X. Zhang, L. Yang, S. Chen, Y. Xu, H. Tang, B. Zhang, H. Wang, Nano-sized PtRu/C electrocatalyst with separated phases and high dispersion improves electrochemical performance of hydrogen oxidation reaction, Front. Chem. 10 (2022) 885965, https://doi.org/10.3389/fchem.2022.885965.
[32] S.A. Stern, The “barrer” permeability unit, J. Polym. Sci. 2 Polym. Phys. 6 (11) (1968) 1933–1934, https://doi.org/10.1002/pol.1968.160061108.
[33] E.J. Park, C.G. Arges, H. Xu, Y.S. Kim, Membrane strategies for water electrolysis, ACS Energy Lett. (2022) 3447–3457, https://doi.org/10.1021/acsenergylett.2c01609.
[34] J. Choi, J.H. Yeon, S.H. Yook, S. Shin, J.Y. Kim, M. Choi, S. Jang, Multifunctional nafion/CeO2 dendritic structures for enhanced durability and performance of polymer electrolyte membrane fuel cells, ACS Appl. Mater. Interfaces 13 (1) (2021) 806–815, https://doi.org/10.1021/acsami.0c21176, 01/13 2021.
[35] D.C. Giancoli, Physics: Principles with Applications, vol. 1, Pearson, 2014.
[36] S. Slade, S.A. Campbell, T.R. Ralph, F.C. Walsh, Ionic conductivity of an extruded nafion 1100 EW series of membranes, J. Electrochem. Soc. 149 (12) (2002), https://doi.org/10.1149/1.1517281.
[37] T. Soboleva, Z. Xie, Z. Shi, E. Tsang, T. Navessin, S. Holdcroft, Investigation of the through-plane impedance technique for evaluation of anisotropy of proton conducting polymer membranes, J. Electroanal. Chem. 622 (2) (2008) 145–152, https://doi.org/10.1016/j.jelechem.2008.05.017.
[38] J. Peron, A. Mani, X. Zhao, D. Edwards, M. Adachi, T. Soboleva, Z. Shi, Z. Xie, T. Navessin, S. Holdcroft, Properties of Nafion® NR-211 membranes for PEMFCs, J. Membr. Sci. 356 (1–2) (2010) 44–51, https://doi.org/10.1016/j.memsci.2010.03.025.

[39] D. DeBonis, M. Mayer, A. Omosebi, R.S. Besser, Analysis of mechanism of Nafion ® conductivity change due to hot pressing treatment, Renew. Energy 89 (2016) 200–206, https://doi.org/10.1016/j.renene.2015.11.081.
[40] Q. Meyer, N. Mansor, F. Iacoviello, P.L. Cullen, R. Jervis, D. Finegan, C. Tan, J. Bailey, P.R. Shearing, D.J.L. Brett, Investigation of hot pressed polymer electrolyte fuel cell assemblies via X-ray computed tomography, Electrochim. Acta 242 (2017) 125–136, https://doi.org/10.1016/j.electacta.2017.05.028.
[41] M. Adachi, T. Navessin, Z. Xie, F.H. Li, S. Tanaka, S. Holdcroft, Thickness dependence of water permeation through proton exchange membranes, J. Membr. Sci. 364 (1–2) (2010) 183–193, https://doi.org/10.1016/j.memsci.2010.08.011.
[42] M. Fumagalli, S. Lyonnard, G. Prajapati, Q. Berrod, L. Porcar, A. Guillermo, G. Gebel, Fast water diffusion and long-term polymer reorganization during nafion membrane hydration evidenced by time-resolved small-angle neutron scattering, J. Phys. Chem. B 119 (23) (Jun 11 2015) 7068–7076, https://doi.org/10.1021/acs.jpcb.5b01220.
[43] V.A. Paganin, E.A. Ticianelli, E.R. Gonzalez, Fabrication and evaluation of electrodes for polymer electrolyte fuel cells, ECS Proceedings Volumes 1995–23 (1) (1995) 102–114, https://doi.org/10.1149/199523.0102pv.
[44] K. Christmann, K.A. Friedrich, N. Zamel, Activation mechanisms in the catalyst coated membrane of PEM fuel cells, Prog. Energy Combust. Sci. 85 (2021), https://doi.org/10.1016/j.pecs.2021.100924.
[45] T. Suzuki, H. Tanaka, M. Hayase, S. Tsushima, S. Hirai, Investigation of porous structure formation of catalyst layers for proton exchange membrane fuel cells and their effect on cell performance, Int. J. Hydrogen Energy 41 (44) (2016) 20326–20335, https://doi.org/10.1016/j.ijhydene.2016.09.078.
[46] A. Kongkanand, M.F. Mathias, The priority and challenge of high-power performance of low-platinum proton-exchange membrane fuel cells, J. Phys. Chem. Lett. 7 (7) (2016) 1127–1137, https://doi.org/10.1021/acs.jpclett.6b00216.
[47] G. De Moor, N. Charvin, C. Bas, N. Caqué, E. Rossinot, L. Flandin, In situ quantification of electronic short circuits in PEM fuel cell stacks, IEEE Trans. Ind. Electron. 62 (8) (2015) 5275–5282, https://doi.org/10.1109/TIE.2015.2395390.
[48] C. Klose, T. Saatkamp, A. Münchinger, L. Bohn, G. Titvinidze, M. Breitwieser, K.D. Kreuer, S. Vierrath, All-hydrocarbon MEA for PEM water electrolysis combining low hydrogen crossover and high efficiency, Adv. Energy Mater. 10 (14) (2020) 1903995, https://doi.org/10.1002/aenm.201903995.
[49] K. Kreuer, in: W. Vielstich, A. Lamm, H. Gasteiger (Eds.), Handbook of Fuel Cells–Fundamentals, Technology and Applications. Volume 3–Fuel Cell Technology and Applications, J Wiley & Sons, Chichester, UK, 2003.
[50] H.F.M. Mohamed, K. Ito, Y. Kobayashi, N. Takimoto, Y. Takeoka, A. Ohira, Free volume and permeabilities of O2 and H2 in Nafion membranes for polymer electrolyte fuel cells, Polymer 49 (13–14) (2008) 3091–3097, https://doi.org/10.1016/j.polymer.2008.05.003.
[51] E. Endoh, Development of highly durable PFSA membrane and MEA for PEMFC under high temperature and low humidity conditions, ECS Trans. 16 (2) (2008) 1229–1240, https://doi.org/10.1149/1.2981964.
[52] H. Lee, M. Han, Y.-W. Choi, B. Bae, Hydrocarbon-based polymer electrolyte cerium composite membranes for improved proton exchange membrane fuel cell durability, J. Power Sources 295 (2015) 221–227, https://doi.org/10.1016/j.jpowsour.2015.07.001.
[53] L. Gubler, W.H. Koppenol, Kinetic simulation of the chemical stabilization mechanism in fuel cell membranes using cerium and manganese redox couples, J. Electrochem. Soc. 159 (2) (2011) B211–B218, https://doi.org/10.1149/2.075202jes.
[54] G.V. Buxton, C.L. Greenstock, W.P. Helman, A.B. Ross, Critical Review of rate constants for reactions of hydrated electrons, hydrogen atoms and hydroxyl radicals (·OH/·O− in Aqueous Solution, J. Phys. Chem. Ref. Data 17 (2) (1988) 513–886, https://doi.org/10.1063/1.555805.
[55] L. Gubler, T. Nauser, F.D. Coms, Y.-H. Lai, C.S. Gittleman, Perspective—prospects for durable hydrocarbon-based fuel cell membranes, J. Electrochem. Soc. 165 (6) (2018) F3100–F3103, https://doi.org/10.1149/2.0131806jes.
[56] V.D.C. Tinh, V.D. Thuc, D. Kim, Chemically sustainable fuel cells via layer-by-layer fabrication of sulfonated poly(arylene ether sulfone) membranes containing cerium oxide nanoparticles, J. Membr. Sci. 634 (2021) 119430, https://doi.org/10.1016/j.memsci.2021.119430, 09/15/2021.
[57] D. Shin, M. Han, Y.G. Shul, H. Lee, B. Bae, Analysis of cerium-composite polymer-electrolyte membranes during and after accelerated oxidative-stability test, J. Power Sources 378 (2018) 468–474, https://doi.org/10.1016/j.jpowsour.2017.12.074. December 2017.